

## Spin Dynamics at the NLC

Ken Moffeit and Mike Woods  
*SLAC*

### Abstract

This note describes spin transport and depolarization effects at the NLC. We also discuss the difference between the polarization measurement by the polarimeter and the luminosity-weighted polarization.

### 1. Introduction

A longitudinally polarized electron beam will be made at the NLC by irradiating a strained GaAs crystal with circularly polarized light with the quantum energy close to the band-gap energy. Electron beam polarization at the source exceeding 80% can be expected. Between the polarized source and the  $e^+e^-$  interaction point the beam is stored in a damping ring, traverses a  $180^\circ$  bend at 8.12 GeV and enters a final focus system as seen in Figure 1. In addition, the beam undergoes severe disruption in the collision process before it is measured at the Compton Polarimeter in the extraction line. It is important to have small polarization losses in the transport and acceleration systems and to minimize spin diffusion.

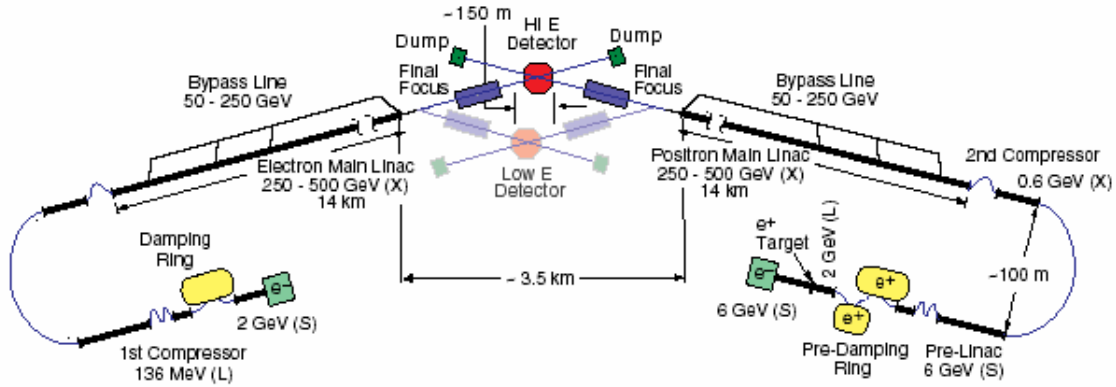


**Figure 1:** Layout of the NLC. [1]

Depolarization comes from both classical (Bargmann-Michel-Telegdi precession: BMT) [2] and quantum (Sokolov-Ternov spin-flip: ST) [3] effects. BMT spin precession with respect to the electron momentum vector is given by:

$$\theta_{spin} = \gamma \frac{g-2}{2} \cdot \theta_{bend} = \frac{E(\text{GeV})}{0.44065} \cdot \theta_{bend} \quad (1)$$

The change in spin direction for various bend angle changes for electron beam energy of 250 GeV is given in Table 1. When there is angular divergence of the beam greater than 100  $\mu\text{rad}$  there will be significant depolarization of the beam.

**Table 1:** Change in spin direction for various bend angles and the projection of the longitudinal polarization. Electron beam energy is 250 GeV.

Change in Bend Angle	Change in Spin Direction	Longitudinal Polarization Projection
1 mrad	32.5°	84.3%
275 $\mu\text{rad}$	8.9°	98.8%
100 $\mu\text{rad}$	3.25°	99.8%

This note describes the spin transport and depolarization effects at the NLC. We also discuss the difference between the polarization measurement by the polarimeter and the luminosity-weighted polarization. A similar discussion of these spin dynamics issues at SLAC and the SLC is given in References [4-7].

**Action item:** give general expression for the spin precession and derive equation 1 and its applicability.

## 2. Spin dynamics in beam transport from source to IR

### 2.1 Injector

Figure 2 shows the electron injector complex layout for the near surface cut-and-cover design of the NLC. The polarized electron source will produce intense pulses of polarized electrons. The longitudinal polarized electrons are accelerated to 1.98 GeV in the front end of the NLC. There are no significant sources of spin diffusion. A possible depolarization discussed by W.K.H. Panofsky and M. Swartz [6] could occur at very low energy less than 50 MeV due to intra-bunch electric and magnetic fields during acceleration in the linac. It was concluded that no serious depolarization occurs and that the effects of the intra-bunch fields are probably undetectable. The NLC injector is similar to that of SLC with some differences: each pulse contained  $5 \cdot 10^{10}$  at SLC while the NLC plans only  $1.6 \cdot 10^{10}$ ; and the Subharmonic Bunchers at SLC were 178.5 MHz, while 714 MHz is planned for NLC. The lower intensity will reduce any depolarization effects at NLC. We do not expect any serious depolarization to occur at the NLC due to this effect.

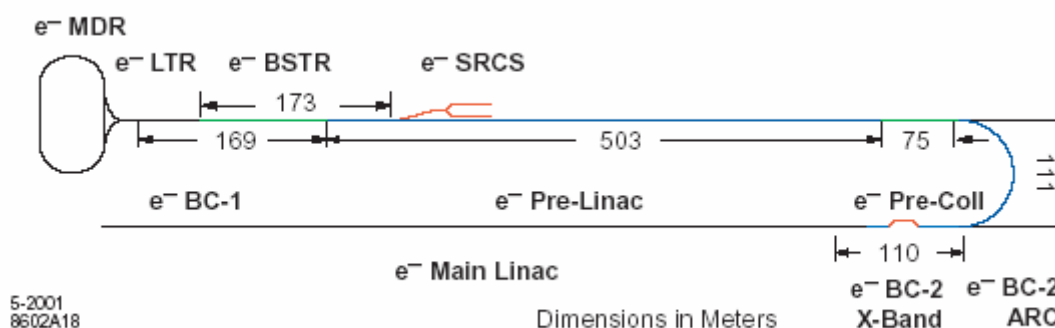


**Figure 2:** Electron injector complex layout for the NLC. The  $e^-$  SRCS is a pair of electron sources;  $e^-$  BSTR is the 2-GeV, S-band booster linac;  $e^-$  LTR is the linac-to-ring transport line;  $e^-$  MDR is the electron main damping ring;  $e^-$  BC-1 is the first stage bunch length compressor; it is followed by the 6-GeV S-band pre-linac;  $e^-$  Pre-Coll is the  $e^-$  pre-collimation region;  $e^-$  BC-2Arc is the second stage bunch length compressor arc; and  $e^-$  BC-2X-band denotes the second compressor stage X-band rf section and magnet chicane.

### 2.2 Damping Rings and Spin Rotators

Electrons, before being compressed and accelerated in the main Linac, are stored for 25 ms in a damping ring (see Figure 3). Only electron spin directions parallel to the magnetic field, that is, transverse to the plane of the damping ring (DR), will preserve their polarization in the DR. A spin rotation system will orient the spin vector parallel to the magnetic field of the damping ring as the electrons traverse the injection line to the ring. At the DR energy of 1.98 GeV, the spin tune,  $\nu_{spin} = \frac{E(\text{GeV})}{0.44065}$ , is 4.5.

The DR will have to be tuned to avoid depolarizing spin resonances, given by

$$\nu_{spin} = k \pm l\nu_x \pm m\nu_y \pm n\nu_s, \quad (2)$$

Where  $k, l, m, n$  are integers;  $\nu_x$  and  $\nu_y$  are the horizontal and vertical betatron tunes and  $\nu_s$  is the synchrotron tune, respectively. The energy spread of the beam (1% full width) and the DR tune spreads have to be sufficiently narrow to avoid the important depolarizing resonances.

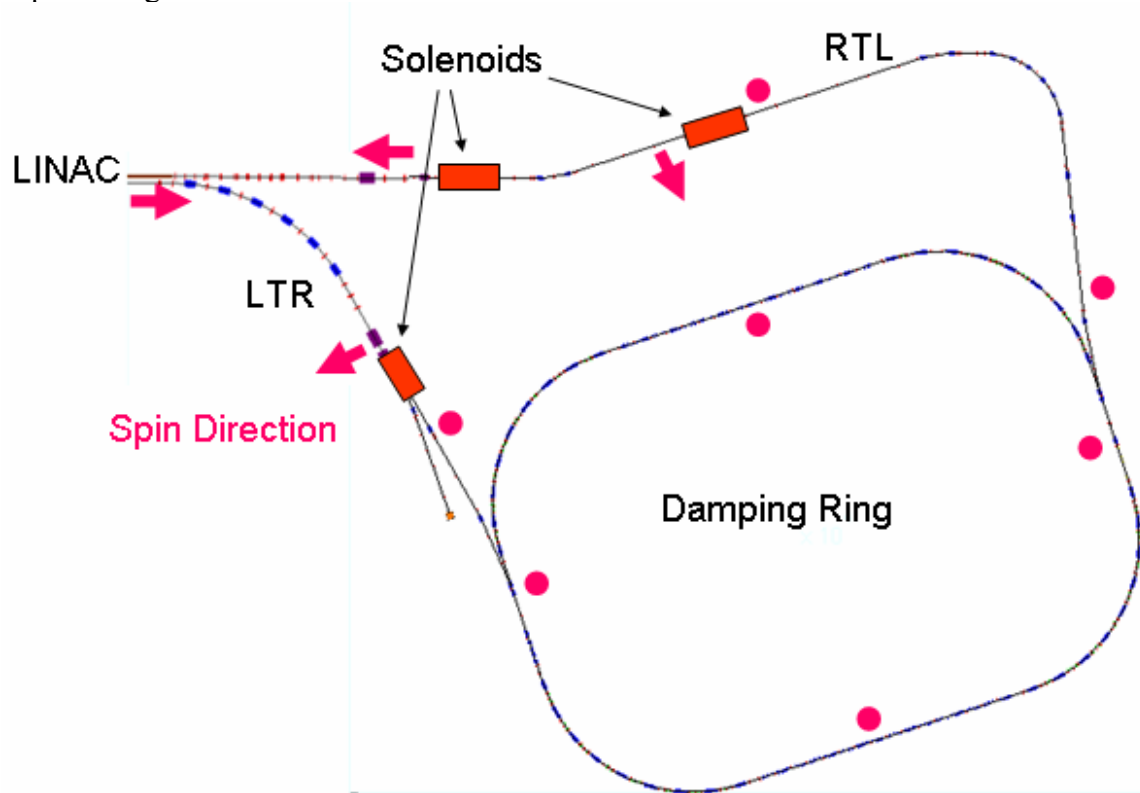


**Figure 3:** Layout of electron damping ring system for the near surface cut-and-cover design of the NLC.

The electrons are longitudinally polarized at the source and during acceleration through the first sector of the linac before being transferred to the DR. At 1.98 GeV, the electron spin component in the plane normal to the applied magnetic field will precess  $90^\circ$  in that plane for every  $20.03^\circ$  of rotation of the momentum vector. An axial solenoid field integral of 10.37 Tesla-meters is then needed to rotate the spin parallel to the field of the DR; i.e., by  $90^\circ$ . The solenoids designed for the NLC [8] are 1.5m in length with maximum field strength of  $\pm 38.5 \cdot kGauss$ ; each will rotate the spin by  $45^\circ$  at a beam energy of 2.2 GeV. In the linac-to-ring (LTR) transfer line the paired solenoids will be located after a bend of  $3 \times 20.03^\circ$ . Following the DR two additional spin rotator systems are needed to achieve arbitrary spin orientation in the Linac or at the IP. To establish longitudinal polarization in the Linac after the DR, one solenoid pair will be installed in the ring-to-linac (RTL) transfer line and the in-plane precession will be accomplished by a subsequent bend of  $20.03^\circ$ . A Linac solenoid pair, located at the beginning of the Pre-Linac, can be used to give arbitrary transverse polarization to the beam – in this case the LTR spin rotators will be powered, while the RTL spin rotators will be off. To achieve full longitudinal polarization at the IP, and to compensate for the spin precession in the

180-degree compressor arc, requires all 3 sets of spin rotators. The procedure for optimizing their settings is described in Section 5. There can be small depolarization effects in and out of the DRs since there may be small energy differences either within a single bunch or along the bunch train. The rotation by the superconducting solenoid into the vertical is  $90^\circ$  only at one energy and electrons with energies higher or lower will not be in the normal to the plane of the DR. Depolarization losses due to this effect are negligible since the entire envelope has a single bunch energy spread of  $\frac{\delta E}{E} = 1\%$  full width and the energy variations along the train are also below 1% [1,9].

### 2.3 Bunch Compressors and 180-degree Arc

The low energy bunch compressor follows the spin rotators. Because there is no net bending there is no depolarization effect.

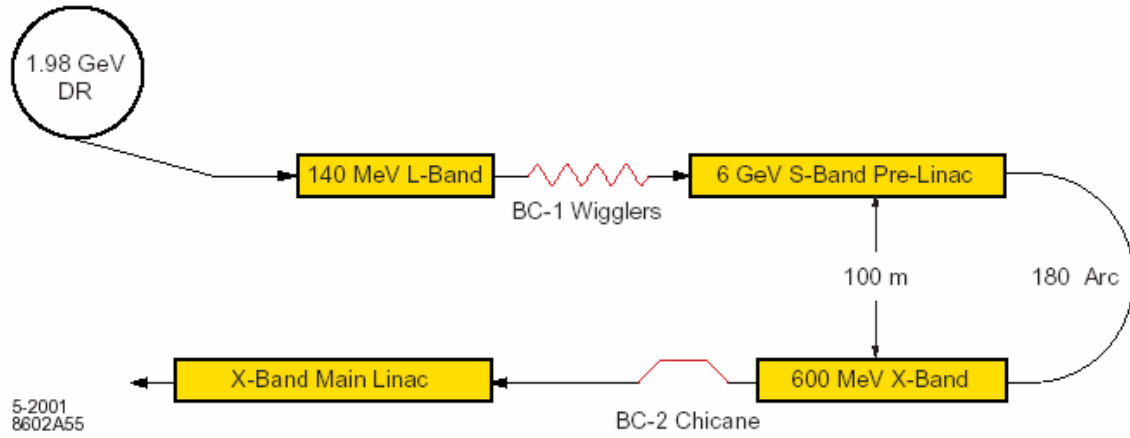


**Figure 4:** Schematic of the NLC bunch compressor system.

The second bunch compressor at 8.12 GeV includes an  $180^\circ$  arc as seen in Figure 4. (Solenoid spin rotators cannot be used at 8 GeV, being limited to low-energy applications due to the necessary scaling of solenoid strength with energy.) These bends will rotate a non-vertically oriented spin vector many times, potentially depolarizing the beam due to the incoming energy spread. A calculation of this depolarization shows it to be small at the level of 1%. Using equation (1) with  $E=8.12$  GeV the reverse bend result in the spin vector to be rotated 9.2 turns. An electron with energy offset

$\delta = \frac{E - 8.12 \text{ GeV}}{8.12 \text{ GeV}}$  will have a polarization projected onto the direction of the bunch's

average spin vector with magnitude  $P(\delta) = P_0 \cos\left(\frac{E}{0.44065} \cdot \delta \cdot \pi\right)$ . The mean

polarization over a beam with a Gaussian energy spread  $\sigma_\delta$  is

$$\bar{P} = P_0 \cdot \frac{1}{\sqrt{2\pi}} \sigma_\delta \int_{-\infty}^{\infty} e^{-\delta^2/2\sigma_\delta^2} \cos\left(\frac{E}{0.44065} \delta \pi\right) d\delta = e^{-\frac{1}{2} \left(\frac{E}{0.44065} \pi \sigma_\delta\right)^2} \quad (2)$$

For an energy spread of  $\sigma_\delta = 0.25\%$  in the 8.12 GeV  $180^\circ$  arc, the relative depolarization is 1.04%.[8]

## 2.4 Linac and Beam Delivery

Electrons are accelerated to 250 GeV in the Main Linac. Spin precession and depolarization effects have been considered previously for the SLAC Linac, including for SLC operation. These are summarized in References [6] and [7] and were found to give less than 0.1% depolarization. At NLC, we also expect depolarization effects in the Linac to be below 0.1%.

After the main Linac, the Beam Delivery system transports the electrons through an energy collimation region to the Final Focus, where they are brought into collision with the opposing positron beam at the interaction point (IP). The net angle between the Linac and the IP is 1 mrad (see Figure 8), causing the spin to precess by 567 mrad between these two locations; this will be compensated for in the spin alignment procedures described in section 5. The energy spread of 0.3%, together with this spin precession, results in much less than 0.1% depolarization due to spin diffusion.

In contrast to the small depolarization effects for the Beam Delivery system at NLC, there were significant spin diffusion effects in the SLC Beam Delivery.[4, 10] This came about from the very large 90-degree Arc bend between the Linac and IP at SLC, which caused a significant spin diffusion from the finite energy spread. (The SLC Arc also operated near a spin tune resonance. 23 achromats, each of which consisted of 20 combined function magnets, comprised the SLC arc. At 46.6 GeV beam energy, the spin precession in each arc achromat was  $1085^\circ$ , very close to the betatron phase advance of  $1080^\circ$ . Vertical betatron oscillations through the horizontal bends of the achromats could then result in significant vertical spin rotation because of the spin tune resonance and the fact that rotations in  $x$  and  $y$  do not commute.)

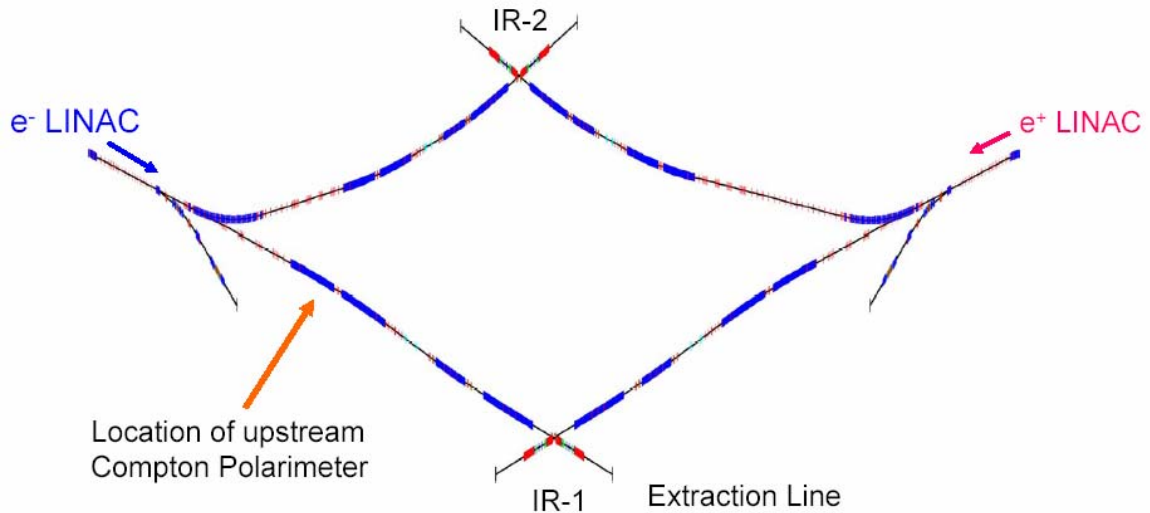


**Figure 5:** Layout of the Beam Delivery System to two Interaction Regions.

Action item: discuss in more detail Linac depolarization issues discussed in References [6] and [7].

Action item: discuss effects for IR-2 with 30-mrad crossing angle (Figure 5)

### 3. Spin precession and depolarization in the Interaction Region

For depolarization effects in the IR, it is important to distinguish between the depolarization for the outgoing beam to the extraction line and the luminosity-weighted depolarization. This is discussed in the relevant sections below. For nomenclature, we use  $\Delta P$  to refer to the depolarization for the outgoing beam from the IP after the beam-beam collision, and we use  $\Delta P^{\text{lum-wt}}$  to refer to the luminosity-weighted depolarization.

#### 3.1 Beam jitter.

Beam jitter at the IP can result in spin precession and an effective depolarization, but the effect is small. Figure 6 shows the vertical deflection angle as a function of the offset of the beams at the interaction point. The expected beam position jitter gives  $\Delta_{\text{Offset}} \approx 0.5\sigma_y$  or about 2nm, which would cause a deflection angle of  $\sim 20 \mu\text{rad}$  for the outgoing beam to the extraction line. At 250 GeV this gives a change in the spin direction of only 11 mrad and a small contribution to  $\Delta P \ll 0.1\%$ . The effect on the luminosity-weighted polarization is even smaller since the luminosity-weighted deflection angle from beam position jitter is only  $\sim 1/2$  of the  $20 \mu\text{rad}$  angle for the outgoing beam. Spin precession effects from incoming angle jitter (expected jitter is  $\sim 1/2$  of the incoming angular divergences) are a little larger, but still a small effect (sub-0.1% contribution to  $\Delta P^{\text{lum-wt}}$ ) because of the small incoming angular divergences (see Table 2).

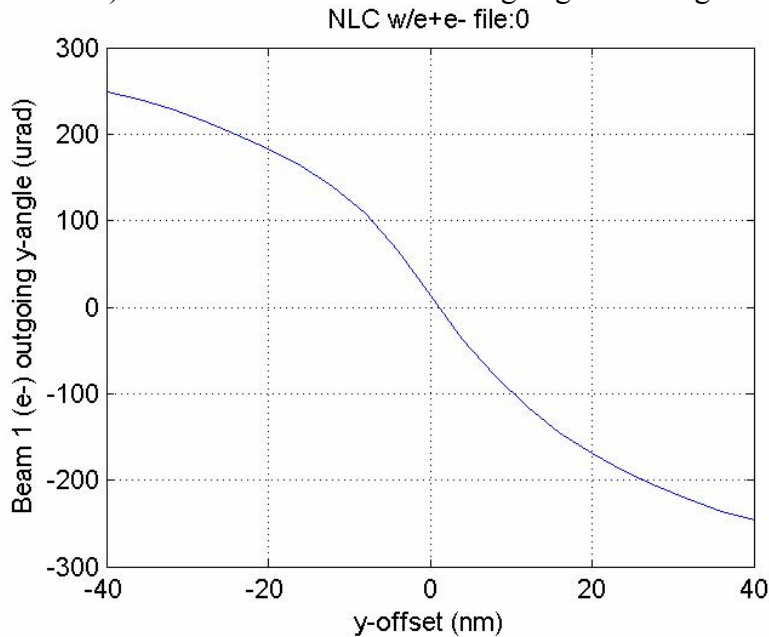


**Figure 6:** Beam deflection scan. The vertical deflection angle is plotted versus vertical offset. [11]

### 3.2 Angular divergences and spin precession at the IP.

Depolarization resulting from spin diffusion is given by:

$$\Delta P^{BMT} = \langle 1 - \cos \theta_{spin} \rangle \quad (3)$$

At the IP, as seen in Table 2, the incoming beams have small angular divergence (<40  $\mu\text{rad}$  rms in each plane) and the resulting  $\Delta P_{IP}^{BMT}$  is negligible. However, the outgoing angular divergences are significantly larger, which results in  $\Delta P_{IP}^{BMT} \approx 1.0\%$  for the outgoing beam to the extraction line. The luminosity-weighted depolarization is smaller, however, and is typically about  $\frac{1}{4}$  of the outgoing beam depolarization because the luminosity-weighted angular divergence of the disrupted beams is typically  $\sim 1/2$  of the angular divergence for the outgoing beam.

**Table 2:** Extraction Line Beam Properties: angular divergences of the incoming and disrupted beams at the NLC IP; BMT depolarization due to the angular divergences. Results are averaged over 6 TRC files. [12]

Parameter	$e^+e^-$
$\sigma(\theta_x)^{in}$	40 $\mu\text{rad}$
$\sigma(\theta_y)^{in}$	25 $\mu\text{rad}$
$\sigma(\theta_x)^{out}$	230 $\mu\text{rad}$
$\sigma(\theta_y)^{out}$	85 $\mu\text{rad}$
$\Delta P_{IP}^{BMT}$	1.0%

### 3.3 Sokolov-Ternov spin flips.

Depolarization of the outgoing beams at the IP can result both from BMT spin precession and from Sokolov-Ternov spin flips from beam-beam effects, [13,14]

$$\Delta P_{IP} = \Delta P_{IP}^{BMT} + \Delta P_{IP}^{ST} \quad (4)$$

The luminosity-weighted depolarization is smaller, however, and is typically about  $\frac{1}{4}$  of the outgoing beam depolarization [13, 14] (whether due to BMT spin precession or due to ST spin flips),

$$\Delta P_{IP}^{lum-wt} = \Delta P_{IP}^{lum-wt,BMT} + \Delta P_{IP}^{lum-wt,ST} \quad (5)$$

$$\Delta P_{IP}^{lum-wt} \approx \frac{1}{4} (\Delta P_{IP}^{BMT} + \Delta P_{IP}^{ST}) \quad (6)$$

At NLC-500, calculations in Reference [14] estimate  $\Delta P_{IP}^{ST} \approx 0.4\%$  and  $\Delta P_{IP}^{lum-wt,ST} \approx 0.1\%$ .

**Action item:** update estimates for  $\Delta P_{IP}^{ST}$  with more recent NLC-500 parameters

### **3.4 Spin Precession from an IP Crossing Angle**

The NLC design has a 20-mrad horizontal crossing angle between the two beams at the IP so that the beams do not influence one another, and the outgoing beam can exit through a beam pipe with a larger aperture than the incoming beam line. Figure 7 shows a schematic of a beam passing through a solenoid with a horizontal crossing angle; the beam trajectories have an angle of 10 mrad with respect to the detector solenoid field. This results in a vertical kick to the beams. The vertical kick from the solenoid in the barrel region of the LC detector is partially cancelled by the compensation kick in the endcap fringe field. In one study of this effect for NLC with 250 GeV beams [15], the deflection angle with respect to the incoming beam trajectory is 100  $\mu\text{rad}$  at the interaction point and 200  $\mu\text{rad}$  for the outgoing beam to the extraction line. These vertical deflection angles are energy dependent,

$$\theta_y^{IP} = 100 \mu\text{rad} \cdot \frac{250\text{GeV}}{E} \quad (10)$$

$$\theta_y^{\text{extraction}} = 200 \mu\text{rad} \cdot \frac{250\text{GeV}}{E}. \quad (11)$$

The vertical bend angles will cause spin precession and misalignment of the spin direction between the collider IP and the Compton IP, for both upstream and downstream Compton polarimeters. The spin angle misalignment between the collider IP and the polarimeter IP will be 56.7 mrad, resulting in 0.14% loss in longitudinal polarization at the collider IP if the spin is oriented at the polarimeter IP. This is small and can be partially corrected for, but is undesirable. There are other undesirable consequences of an uncompensated solenoid with a crossing angle at the IP: for  $e^-e^-$  collisions there would be a vertical crossing angle, and alignment of the extraction line would be energy-dependent. A recent proposal [15] for compensating the crossing-angle/solenoid vertical steering uses a serpentine winding for the solenoid so that the orbit at the IP has no offset or angle with respect to the incoming beam trajectory. This still leaves an offset/angle for the outgoing beam to the extraction line which will be corrected with an external dipole. One dipole would be sufficient to correct the angle, but two are needed to correct position and angle. A dipole for just the angle would be located at  $z=6$  meters after the IP.

## **4. Polarimeters**

We plan to measure the electron polarization using two Compton polarimeters: one located 1034 meters upstream of the IP for the incoming electron beam and a second one 60 meters downstream of the IP in the extraction line.

Figure 8 shows the transport line for the final focus. The upstream Compton polarimeter is located before the energy-slit where the direction of the beam is the same as that at the IP. The dispersion and beta functions in the region of the upstream polarimeter are shown in Figure 9. There is a bend angle of 0.35 mrad between the Compton IP and the energy slits which can be used as a spectrometer for the Compton-scattered electrons. The design of this region to incorporate a Compton Polarimeter is in progress.

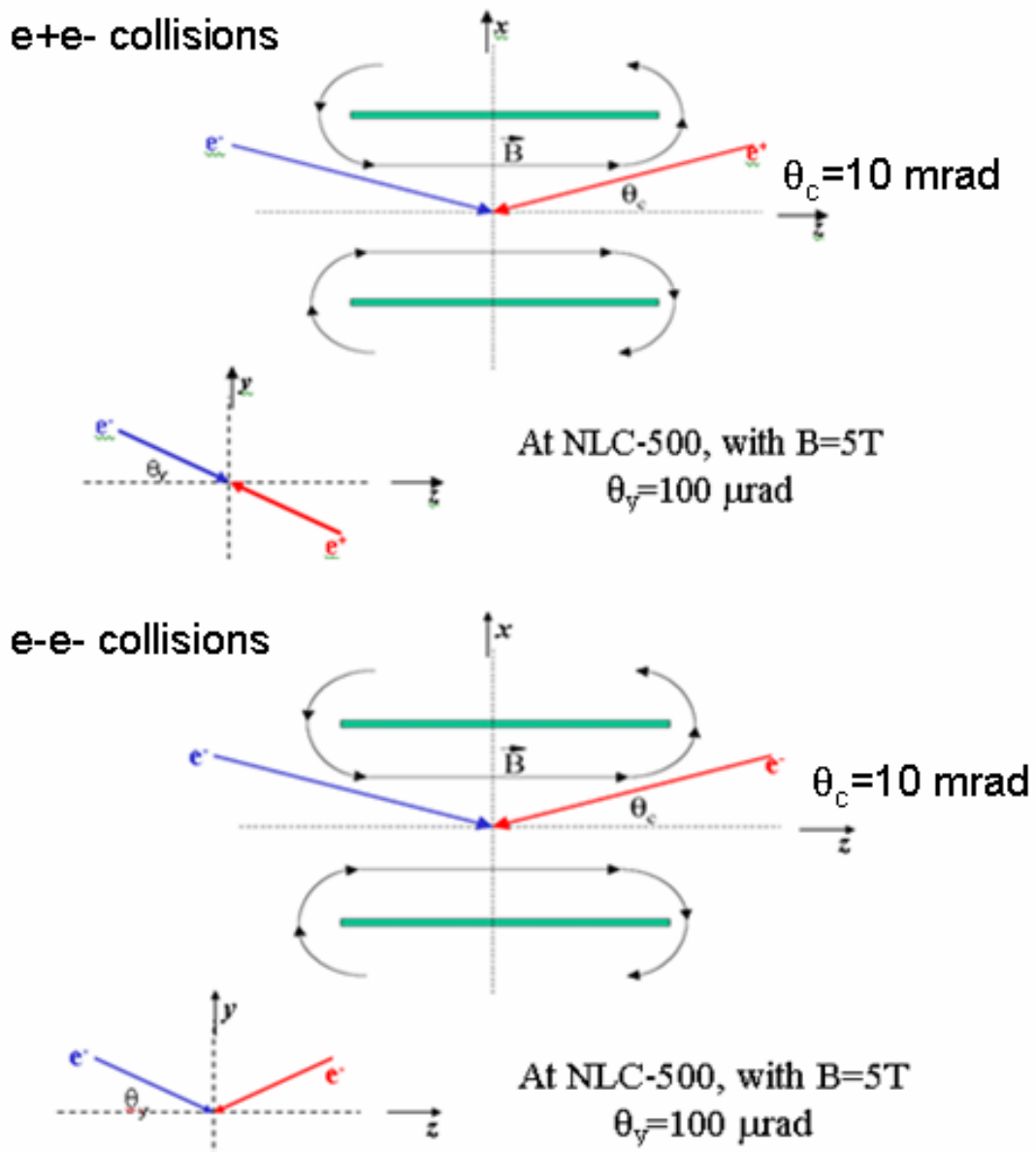


**Figure 7:** Schematic of a beam passing through a solenoid with a horizontal crossing angle for  $e^+e^-$  collisions (top) and  $e^-e^-$  interactions (bottom).

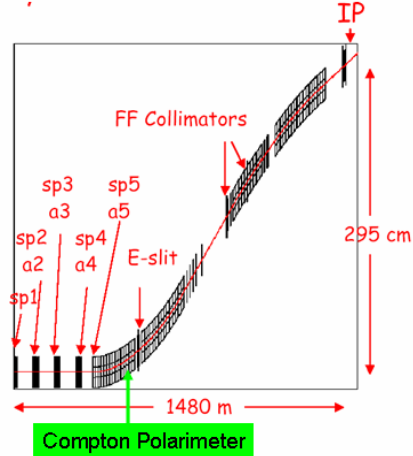


**Figure 8:** The electron beam final focus showing the collimators and the energy slit. The upstream Compton polarimeter to measure the electron beam polarization before collision is located before the E-slit (1034 meters upstream of the IP) where the direction of the beam is the same as that at the IP.[16]

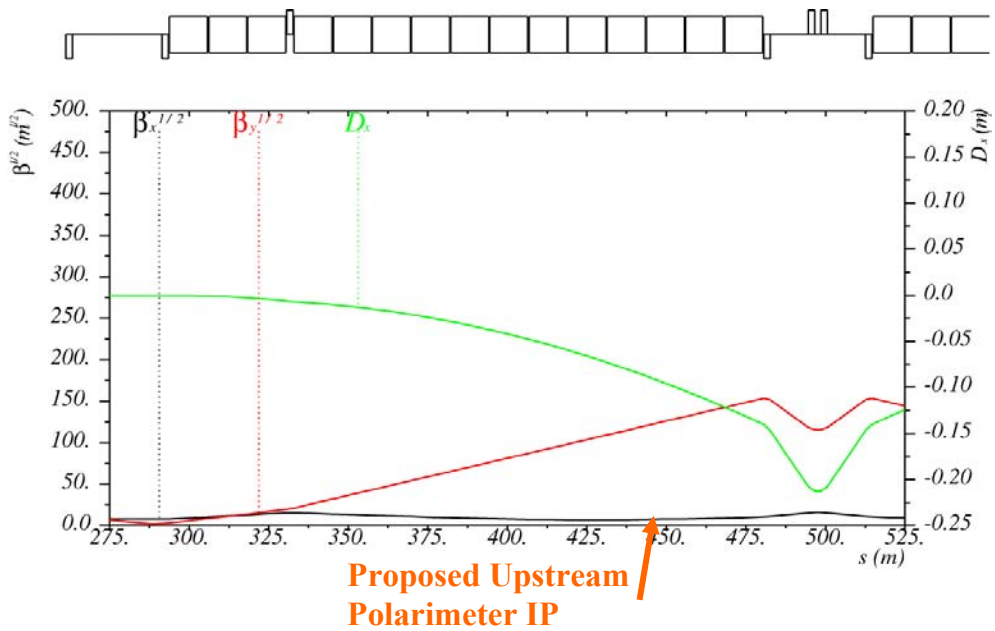


**Figure 9:** Beta-functions and dispersion in the region of the proposed upstream polarimeter location as a function of distance from end of the Linac.[16]

The location of the downstream Compton Interaction Point in the extraction line is shown in Figures 10 and 11. It is at a secondary focus in the middle of a chicane with 20 mm dispersion, but with no net bend angle with respect to the electron beam direction at the primary  $e^+e^-$  interaction point [17]. At the middle of the chicane the Compton scattering will occur and the scattered electron is confined to a cone having a half-angle of  $\theta = 2 \mu\text{rad}$  and is effectively collinear with the initial electron direction.

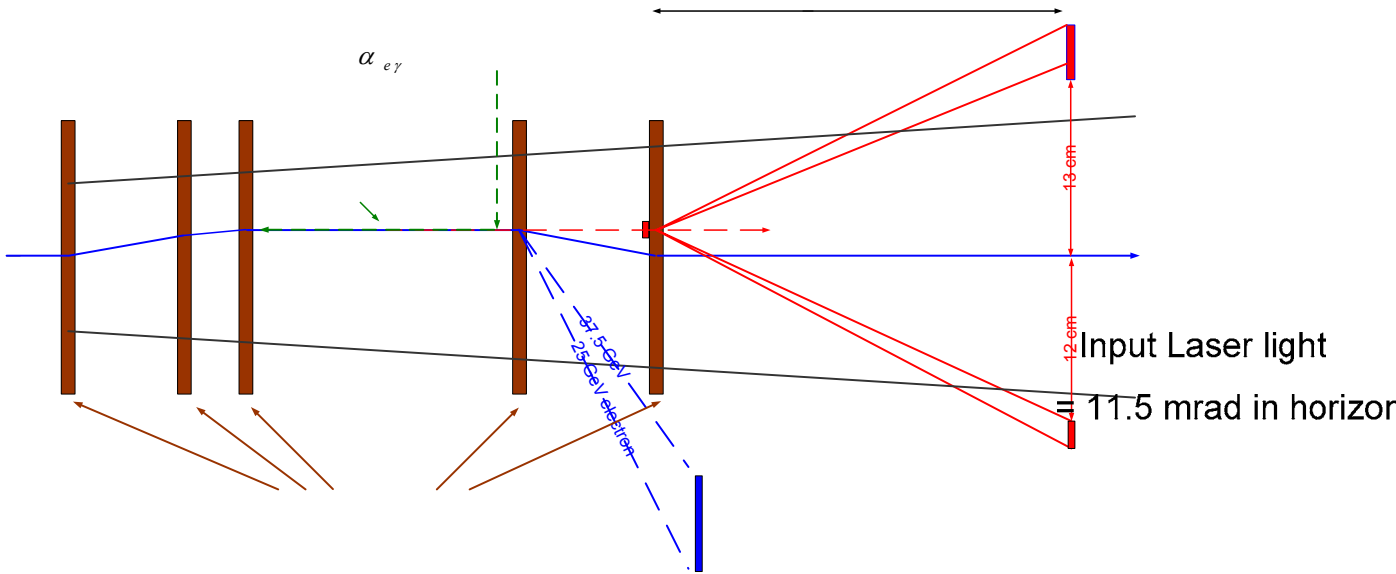


**Figure 10:** System layout showing the Chicane bend magnets, Compton IP, and Compton electron detector.

The R-Transport matrix from the Compton IP to the extraction line Compton IP allows one to compare the beam parameter phase space between the two locations,

$$|x\rangle_{chicane} = R|x\rangle_{IP} \quad (8)$$

This matrix can be determined from the beam optics. The current R-Transport matrix for the NLC extraction line from the IP to the chicane is:

$$R = \begin{pmatrix} -1.68 & 0 & 0.012 & 0 & 0 & 0 \\ 0.0056 & -0.595 & 0 & 0.004 & 0 & 0 \\ -0.016 & 0 & -2.26 & 0 & 0 & 0.02 \\ 0 & -0.003 & -0.099 & -0.443 & 0 & 0 \\ 0 & 0 & -0.002 & -0.009 & 1 & 0 \\ 0 & 0 & 0 & 0 & 0 & 1 \end{pmatrix} \quad (9)$$

for beam parameters  $(x, x', y, y', z, dE/E)$  with units (m, radians, m, radians, m, dimensionless). The angular magnification for both horizontal and vertical is close to -0.5.

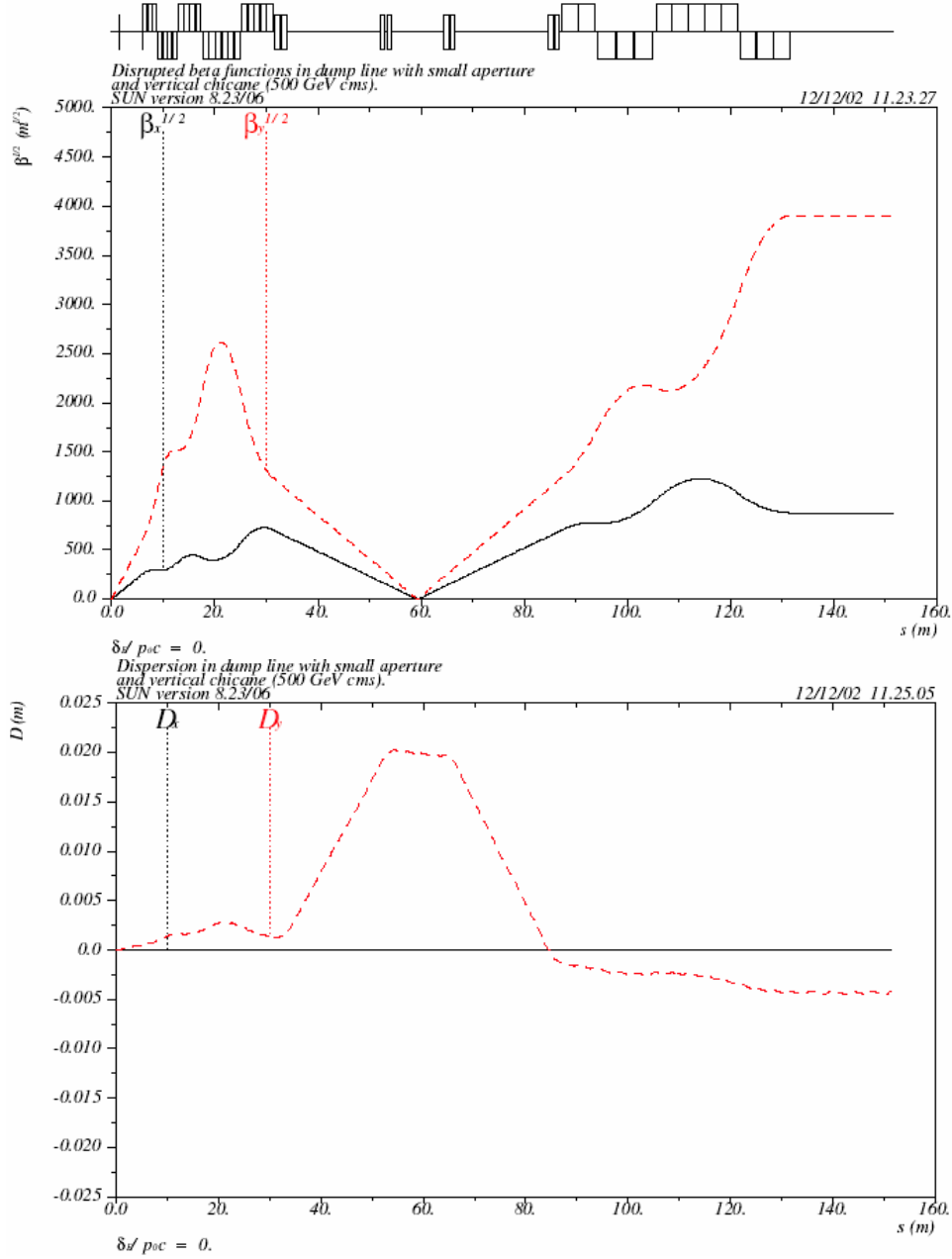


**Figure 11:** Beta-functions and dispersion in the extraction line as a function of distance from the IP. The Compton IP will be located at the secondary focus approximately 60 meters downstream.

One important feature of the extraction line Compton polarimeter is that it can be used to measure the difference in polarization between collisions and no collisions. The depolarization at the Compton IP has contributions from both BMT spin precession and Sokolov-Ternov spin flips:

$$\Delta P_{CIP}^{meas} = \Delta P_{CIP}^{BMT} + \Delta P_{IP}^{ST} . \quad (7)$$

$\Delta P_{CIP}^{BMT}$  can differ from  $\Delta P_{IP}^{BMT}$  due to the R-Transport matrix between the IP and the CIP. The current NLC extraction line has an angular magnification from the IP to the CIP close to -0.5, so that  $\Delta P_{CIP}^{BMT} \approx \Delta P_{IP}^{lum-wt,BMT}$ . If the disrupted beam angles can be determined (from simulations or from extraction line measurement) then one can infer both  $\Delta P_{IP}^{BMT}$  and  $\Delta P_{CIP}^{BMT}$ . The extraction line measurement of  $\Delta P_{CIP}^{meas}$  can then be used to determine  $\Delta P_{IP}^{ST}$ . For example, Reference [12] studied one of the (TRC) NLC-500 files and found that  $e^+e^-$  collisions gave  $\Delta P_{IP}^{lum-wt,BMT} = 0.22\%$ . The R-Transport matrix to the Compton IP predicted that the disrupted beam would have  $\Delta P_{CIP}^{BMT} = 0.31\%$ . Using a GEANT-3 simulation to transport the disrupted electron beam to the CIP and applying a weighting for the collision with the Compton laser beam the study found  $\Delta P_{CIP}^{BMT} = 0.28\%$ , in good agreement with the predicted value from the R-Transport matrix.

**Action item:** what are possibilities for an upstream polarimeter for IR2?

## 5. Spin Alignment Procedures

The procedure for setting the spin direction so the electrons are longitudinally polarized at the IP is as follows:

- Accurate beamline and quad alignment is needed to achieve  $< \sim 10$ urad orbit tolerance between the IP and either upstream or downstream polarimeter locations.
- Obtain reference orbit through the extraction line with solenoid off and with electron-beam only (no collisions).
- Optimize spin rotator settings with solenoid off. Perform a “3-state measurement” with each of  $x$ ,  $y$  and  $z$  spin orientation in the Linac: measure the longitudinal spin component at each of the upstream/downstream polarimeters for each of the 3 spin orientations. The  $z$ -component of the spin transport matrix,  $S$ , between the Linac and the polarimeter can then be determined using

$$P_z^{polarimeter} = S_{zx} \cdot P_x^{Linac} + S_{zy} \cdot P_y^{Linac} + S_{zz} \cdot P_z^{Linac} .$$

This determines the (unitary) spin transport matrix. It can be inverted to determine the optimal RTL and LINAC spin rotator settings to achieve longitudinal spin at the polarimeter.

- Scan each individual spin rotator about optimal to check or fine tune the settings.
- Turn on the solenoid and serpentine/dipole compensation and reproduce the extraction line orbit. Then repeat the spin rotator optimization procedure described in steps above.

- Analysis of this data should verify the relative alignment of the upstream and downstream polarimeters and determine the uncertainties in orbit and spin alignment between the polarimeters and the IP.

We expect to achieve 25 mrad tolerances for the orientation of the spin at either the upstream or downstream polarimeters via the procedure described above. Additionally, we expect to achieve a tolerance of 50  $\mu\text{rad}$  for the orbit between the IP and either polarimeter, with the IR solenoid off; the largest uncertainty comes from the orbit through the Interaction Region. Lastly, we expect to compensate the crossing angle/solenoid steering effects to better than 10%.

## 6. Differences between polarimeter measurement and the luminosity-weighted Polarization.

We define the difference between the luminosity-weighted polarization and the Compton polarization measurement to be  $dP = P_z^{IP, lum-wt} - P_z^{polarimeter}$ . We assume that the spin alignment procedure just described in Section 5 will be used to fully align the electron beam's longitudinal spin at either the upstream or downstream polarimeter IP location. (In practice we expect to achieve this spin alignment with a precision of 25 mrad. Spin misalignment from non-optimal spin rotator settings will be common between the polarimeter IP and the collider IP, but will give a small increase to  $dP$  and the associated systematic error in determining  $dP$ .)

### 6.1 Orbit misalignment between IP and polarimeter.

An orbit misalignment between the IP and polarimeter will cause a contribution to  $dP$ . The rms alignment tolerances are expected to be  $<50 \mu\text{rad}$  between the collision IP and the polarimeter IP, for either the upstream or downstream polarimeter. At 250 GeV this gives a change in the spin direction  $<28 \text{ mrad}$  and is a small effect on the longitudinal polarization projection. Assuming full longitudinal spin alignment at the polarimeter, a 28 mrad spin rotation at the collider IP would give a contribution  $dP = -0.04\%$ .

### 6.2 Compensation for solenoid/crossing angle steering effect.

The uncompensated angle between the upstream polarimeter and the collider IP is 100  $\mu\text{rad}$  as discussed in Section 3.4; it is expected to be compensated to an accuracy of  $\sim 10 \mu\text{rad}$ , resulting in  $<0.01\%$  difference between the upstream polarimeter measurement and the polarization at the IP.

The uncompensated angle between the downstream polarimeter and the collider IP is 200  $\mu\text{rad}$  as discussed in Section 3.4; it is expected to be compensated to an accuracy of  $\sim 30 \mu\text{rad}$ , resulting in a contribution  $dP = -0.01\%$ , assuming the spin is fully aligned at the downstream polarimeter.

### 6.3 Sokolov-Ternov spin flips.

Reference [14] calculated the depolarization at the IP from S-T spin flips to be  $\Delta P^{ST} = 0.4\%$  and  $\Delta P^{lum-wt, ST} = 0.1\%$  for an earlier (circa 2000) set of NLC parameters with

center-of-mass energy 500 GeV. This would contribute  $dP=-0.1\%$  for upstream polarimetry and  $dP=+0.3\%$  for downstream polarimetry.

#### **6.4 Angular divergences and BMT spin precession.**

The incoming angular divergences at the collider IP are 40  $\mu\text{rad}$  rms horizontal and 25  $\mu\text{rad}$  rms vertical. This results in  $\sim 0.03\%$  depolarization due to spin diffusion at the IP. The beam angular divergences at the polarimeter IP locations are much smaller and the corresponding spin diffusion is negligible. Hence, incoming angular divergences contribute  $dP=-0.03\%$ .

The disrupted angular divergences at the collider IP are significant with the outgoing beam from the IP having a horizontal rms angular divergence of 230  $\mu\text{rad}$  and a vertical rms angular divergence of 85  $\mu\text{rad}$ . This contributes a luminosity-weighted depolarization at the IP of 0.25%. The outgoing beam to the extraction line has a larger depolarization due to this effect of 1.0%, but one has to take into account the R-Transport matrix from the IP to the downstream polarimeter IP to calculate the angular divergence and depolarization from spin diffusion there. This was discussed in Section 4 where it was found that spin diffusion from beam-beam disruption gave 0.1% larger depolarization at the extraction line polarimeter IP than at the collider IP.

#### **6.5 Chromatic Aberrations**

Chromatic aberrations at the SLC, together with a finite energy spread and the large spin precession in the SLC Arcs, gave a significant contribution to  $dP$ . In the final SLD physics run, this gave a contribution  $dP=+0.1\%$ . For NLC, we expect this effect to be negligible.

Action item: Following the 180-degree arc at 8.12 GeV, there is a significant correlation between beam energy and polarization. If this energy-polarization correlation persists at a significant level to the IP, chromatic aberrations in the final focus could then give a contribution to  $dP$ . Need to evaluate this.

## 7. Conclusions

### 7.1 Depolarization.

Table 3 summarizes the electron beam depolarization expected for  $e^+e^-$  collisions at NLC-500. The polarization loss is small and the average polarization delivered to the IR is expected to be ~98.6% of that produced at the polarized source.

**Table 3:** Summary of depolarizing effects.

<b>Region</b>	<b>Luminosity-weighted Depolarization</b>
Injector	<0.1%
Damping Ring	<0.1%
Compressor and Pre-Linac	1.04%
Linac	<0.1%
Beam Delivery	<0.1%
Beam orbit jitter	<0.1%
IP incoming Beam divergence	<0.1%
IP disrupted beam divergence	0.25%
Spin-flips from collisions	0.1%
<b>TOTAL</b>	<b>1.4%</b>

### 7.2 Polarimeter and lum-wted polarization differences.

Spin dynamics effects in the IR can result in the measurement made in the Compton polarimeter being different than the luminosity-weighted polarization at the IP. These effects were discussed in Section 6 and are summarized in Table 4.

Both upstream and downstream polarimeters are desirable. Their redundancy provides both for a cross check of the polarization measurement and better ability to estimate the systematic uncertainty on the luminosity-weighted polarization. The capability of the downstream polarimeter to make measurements both with and without collisions is necessary for a direct measurement of the depolarizing effects due to BMT spin precession and S-T spin flips.

**Action item:** estimate systematic errors for the 3 polarimeter measurements from these effects.

**Table 4:** Differences between the luminosity-weighted polarization and the Compton polarization measurement,  $dP = P_z^{IP, lum-wt} - P_z^{polarimeter}$

Effect	dP (Upstream polarimeter)	dP (Downstream polarimeter; no collisions)	dP (Downstream polarimeter; w/ collisions)
Orbit alignment between IP and polarimeter	-0.04%	-0.04%	-0.04%
Angular Divergence of incoming beam	-0.03%	-0.03%	-0.03%
Angular Divergence of disrupted beam	-0.25%	-0.25%	+0.1%
Uncompensated vertical kick due to solenoid field with 10 mrad crossing angle	<0.01%	-0.01%	-0.01%
Sokolov-Ternov spin flips	-0.1%	-0.1%	+0.3%
Chromatic Aberrations	-	-	-
<b>TOTAL</b>	<b>-0.42%</b>	<b>-0.43%</b>	<b>+0.32%</b>

## References

- [1] 2002 TRC Report, <http://www.slac.stanford.edu/xorg/ilctr/2002/2002/report/PAPERS/TRC03C3.PDF> .
- [2] V. Bargmann, L. Michel, and V.L. Telegdi. *Precession of the polarization of particles moving in a homogeneous electro-magnetic field.* *Phys. Rev. Lett.* 2(10):435-436, 1959.
- [3] A.A. Sokolov, I.N. Ternov, *On Polarization and Spin Effects in the Theory of Synchrotron Radiation*, *Sov. Phys. Doklady* 8, 1203 (1964).
- [4] M. Woods, *The polarized electron beam for the SLAC Linear Collider*, SLAC-PUB-7320, (1996); e-Print Archive: hep-ex/9611006.
- [5] K. Moffeit and R. Prepost, *Polarization between Source and Arc*, SLCPOL Note 7, 1985.
- [6] M. Swartz, *The Panofsky Effect*, SLCPOL Note 39, 1987; W.K.H. Panofsky, *Depolarization (?) in the space charge field of the SLC bunch during acceleration*, SLAC-CN-361, 1987.
- [7] W.K.H. Panofsky, *Spin Motion of Electrons in the SLC Linac*, SLAC-CN-383-REV, 1991; Richard H. Helm and W.P. Lysenko, *Electron Beam Depolarization at SLAC*, SLAC-TN-72-001, 1972.
- [8] Paul Emma, in *Zeroth-order Design Report for the Next Linear Collider SLAC Report 474*, Section 5.3.3, 1996.
- [9] The NLC Collaboration, Nan Phinney, General Editor, *2001 Report on the Next Linear Collider*, SLAC Report 571, pg 83, June 2001.

- [10] P. Emma, T. Limberg and R. Rossmanith, *Depolarization in the SLC Collider Arcs*, SLAC-PUB-6527, 1994.
- [11] Arik Florimonte, private communication, 2004.
- [12] M. Woods, K.C. Moffeit, T.O. Raubenheimer, A. Seryi, C. Sramek, A. Florimonte, *Luminosity, Energy and Polarization studies for the Linear Collider: comparing  $e^+e^-$  and  $e-e^-$  for NLC and TESLA*, SLAC-PUB-10353, IPBI-TN-2004-1 (2004). e-Print Archive: physics/0403037
- [13] K. Yokoya and P. Chen, *Depolarization due to beam-beam interaction in electron-positron Linear Colliders*, SLAC-PUB-4692 (1988); published in Minneapolis Spin Conf. 1988:938
- [14] K.A. Thompson, *Spin depolarization due to beam-beam interaction in NLC*, SLAC-PUB-8716 (2001); published in “Capri 2000, Quantum aspects of beam physics” 450-459.
- [15] B. Parker and A. Seryi, *Compensation of the Effects of Detector Solenoid on the Vertical Beam Orbit in NLC*, LCC-0143. (2004)
- [16] A. Seryi, private communication.
- [17] D. Cinabro, E. Torrence and M. Woods, *Status of Linear Collider Beam Instrumentation Design*, 2003. [IPBI TN-2003-1](#).